International Journal of Pharmaceutics 572 (2019) 118712

Contents lists available at ScienceDirect

International Journal of Pharmaceutics

journal homepage: www.elsevier.com/locate/ijpharm

Lamellar liquid crystals maintain keratinocytes' membrane fluidity: An AFM qualitative and quantitative study

Mirjam Gosenca Matjaž[a], Miha Škarabot[b], Mirjana Gašperlin[a], Biljana Janković[a,*]

[a] University of Ljubljana, Faculty of Pharmacy, Aškerčeva cesta 7, Ljubljana, Slovenia
[b] Jožef Stefan Institute, Department of Condensed Matter Physics, Jamova cesta 39, Ljubljana, Slovenia

ARTICLE INFO

Keywords:
Atomic force microscopy
Lamellar liquid crystals
Keratinocyte
Morphology
Elasticity
Membrane fluidity

ABSTRACT

Despite extensive investigations of lamellar liquid crystals for dermal application, the effects of these systems at the cellular level are still not well elucidated. The key aim of this study was to determine the elasticity and morphological features of keratinocytes after exposure to a lamellar liquid crystal system (LLCS) using atomic force microscopy (AFM) as the method of choice. Prior to AFM assessment, a cell proliferation test and light plus fluorescence imaging were applied to determine the sub-toxic concentration of LLCS. According to the AFM results, slightly altered morphology was observed in the case of fixed keratinocytes, while an intact morphology was visualized on live cells. From the quantitative study, decreased Young's moduli were determined for fixed cells (i.e., 8.6 vs. 15.2 MPa and 1.3 vs. 2.9 MPa for ethanol or PFA-fixed LLCS-treated vs. control cells, respectively) and live cells (i.e., ranging from 0.6 to 2.8 for LLCS-treated vs. 1.1–4.5 MPa for untreated cells), clearly demonstrating increased cell elasticity. This is related to improved membrane fluidity as a consequence of interactions between the acyl chains of cell membrane phosphatidylcholine and those of LLCS. What seems to be of major importance is that the study confirms the potential clinical relevance of such systems in treatment of aged skin with characteristically more rigid epithelial cells.

1. Introduction

Lamellar liquid crystals are acknowledged as ideal dermal delivery systems with advantages inseparably connected to their unique microstructure. Their main and inventible constituents are hydrated or solvated amphiphilic molecules in the shape of cylinders that self-assemble to form a distinctive bilayer structure (Müller-Goymann, 2004), resulting in thermodynamic stability, suitable consistency, and feasible preparation, along with enhanced solubilisation properties and the potential for modified drug release (Makai et al., 2003). Thermodynamic stability makes them superior to more frequently used vehicles like emulsions or liposomes, while suitable rheological properties avoid problems encountered with low viscosity systems such as microemulsions or solid lipid nanoparticles/liposomes dispersions. Moreover, their microstructure closely resembles the intercellular lipid matrix in human stratum corneum (SC) with its unique lamellar arrangement [van Smeden et al., 2014] as well as the cell membrane structure. Novel aspects regarding cell membrane organization are reported in the literature (Goñi, 2014), nevertheless the basic fluid-mosaic model is still relevant (Nicolson, 2014).

Selecting safe amphiphilic molecules in the early stage of development—most often non-ionic (i.e., Tweens) or zwitterionic surfactants of natural origin (i.e., lecithin) together with novel natural surfactants (i.e., alkyl glucoside (Savić et al., 2009) —is one of the crucial aspects in formulating skin-compliant delivery systems with a low risk of (cyto)toxicity. In skin research, keratinocytes are frequently utilized as model cells for *in vitro* cytotoxicity testing being most relevant and accessible, where simultaneous morphological evaluation using various microscopic techniques complementary to biological assays (Gibbs, 2009) provides improved results (Hazen et al., 2010).

The most recent and relevant technique for investigating the fluidizing impact as well as visualizing structural changes in cell membranes is atomic force microscopy (AFM) (Alsteens et al., 2017; Maver et al., 2016). In cell mechanics, AFM provides local imaging of cell membrane structures and precise force measurements in a range of 10^{-5} to 10^{-11} N. For assessment of cell membrane fluidity, the AFM tip is used as a nanoindenter and sensor of the force needed to induce elastic deformation (mapping of cell membrane stiffness). To date, AFM has made possible a superior understanding of keratinocytes' basic characteristics, above all their mechanical properties in correlation to cytoskeletal network elements and adhesion structures (Fung et al. 2010, 2011; Lulevich et al., 2010). However, there is a constant

* Corresponding author.
E-mail address: biljana.jankovic@ffa.uni-lj.si (B. Janković).

https://doi.org/10.1016/j.ijpharm.2019.118712
Received 12 July 2019; Received in revised form 13 September 2019; Accepted 16 September 2019
Available online 05 October 2019
0378-5173/

development of biological cells' mechanics measurements (Sokolov et al., 2013) along with critical appraisal of data in a view of measurement parameters proved to have major impact on results (Garcia and Garcia, 2018; Li et al., 2018). In that regard, AFM has been extensively implemented for studying cancer cell biomechanicals (Coceano et al., 2016; Hayashi and Iwata, 2015; Luo et al., 2016; Zemla et al., 2018).

Worthy of note is also AFM substantial contribution for nanoscale drug delivery systems characterization, e.g., solid lipid nanoparticles along with their effect on cellular morphology (Kristl et al., 2013), nanofibers (Pelipenko et al., 2013), liposomes (Takahashi et al., 2018) or even biological cell based carriers (Drvenica et al., 2016) as reviewed by Sitterberg et al., 2010.

In our previous study, the phase behavior of lecithin/Tween 80/isopropyl myristate/water systems were formulated, and a specific lamellar liquid crystal system (LLCS) was determined to be suitable for dermal application with respect to its composition, its physical properties, and especially its superior biological acceptability (low cytotoxicity) (Gosenca et al., 2013).

This study involves screening of cell proliferation and structural features with regard to the concentration ranges and exposure times of the LLCS selected. As a result, we defined the optimal conditions of cell treatment with LLCS that ensure no interference with the cell's metabolism and morphology prior to AFM measurements of cell elasticity. The impact of the LLCS system investigated on the keratinocyte's membrane structure is revealed for the very first time using the AFM nanoindentation approach. Conceptually, this is a step forward compared to our earlier work because direct visualization of morphological changes and assessment of cell membrane stiffness alteration were assessed. The main question raised for consideration is related to the ability of AFM to detect early changes in cell morphology and stiffness after short-term (i.e., 4 h) exposure to LLCS. Elasticity was evaluated on immobilized and live cells, which provide crucial data about the mechanical resistance of the cell membrane following LLCS treatment.

2. Materials and methods

2.1. Materials

Isopropyl myristate (IPM) and Tween 80® (polyoxyethylene (20) sorbitan monooleate) were obtained from Fluka, Sigma-Aldrich GmbH, Steinheim, Germany. Soybean lecithin (Lipoid S-100®; not less than 94% w/w phosphatidylcholine content) was provided by Lipoid GmbH, Ludwigshafen, Germany. Bidistilled water was used throughout the experiments.

The cell culture reagents and reagents used in cell treatment protocols were from Sigma-Aldrich, Germany unless otherwise indicated.

2.2. Methods

2.2.1. LLCS sample preparation

LLCS, with reported physicochemical properties (Gosenca et al., 2013), was used for cell treatment throughout the study. It was prepared by mixing Tween 80 and lecithin at a mass ratio of 1/1 (45%) with isopropyl myristate (17.50%) and followed by the addition of water (37.50% (w/w)) during continuous stirring.

For cell treatment, LLCS was freshly diluted in cell culture medium prior each experiment and used in final concentrations of 0.5, 1, 2, and 5 mg/ml for cell proliferation assay and fluorescence imaging. In view of obtained results, a concentration of 0.5 mg/ml was chosen as non-cytotoxic and therefore used for all further AFM experiments.

2.2.2. Cell culture

Human keratinocytes (cell line NCTC 2544, ICLLCS, University of Genoa) were grown in Eagle's Minimum Essential Medium with Earle's balanced salt solution supplemented with 1% (v/v) non-essential amino acids, 2 mM L-glutamine, and 100 U/ml antibiotic/antimycotic plus 10% or 15% (v/v) fetal bovine serum (Gibco, Invitrogen, Waltham, MA, USA), respectively. Cells were cultured as adherent monolayers at 37 °C in a humidified atmosphere of 5% CO_2, routinely examined using an inverted light microscope (Olympus CKX41, Tokyo, Japan), and regularly subcultured with trypsin/EDTA when they reached 80–90% confluence.

2.2.3. Cell proliferation assay

The keratinocytes were seeded at a density of 0.5×10^4 cells per well in 96-well plates and left overnight to attach. Afterward the cells were incubated with test formulations for 4 or 24 h; then their proliferation was determined using the MTS assay (Cell Titer 96 Aqueous One Solution Cell Proliferation Assay; Promega, Madison, WI, USA) according to the manufacturer's procedure. The assay is based on conversion of 3–4,5-dimethylthiazol-2-yl)-5-(3-carboxymethoxyohenyl)-2-(4-sulfophenyl)-2H-tetrazolium; inner salt into the soluble colored formazan product by mitochondrial dehydrogenase enzymes in metabolically active cells. Cell proliferation, which indirectly points to the number of viable cells, was determined by measuring the absorbance of formazan at 492 nm using a Safire2 microplate reader (Tecan, Zürich, Switzerland). The cell proliferation was expressed as the absorbance ratio of treated to control cells, minus absorbance of test formulation in cell-free medium and medium alone, respectively. The results of cell proliferation assay are expressed as means ± SD. Statistical analysis was carried out using an independent samples Student's *t*-test. Significance was tested at the 0.05 level of probability.

2.2.4. Fluorescence microscopy

The morphology of the cells was examined using a fluorescent microscope (Olympus IX81, Tokyo, Japan). Fixed-slide samples were prepared. Specifically, cells at a density of 2×10^5 cells per well were plated on square glass cover slips in supplemented medium and incubated in 6-well plates overnight. Following incubation with test formulation for a predetermined time, the medium was removed, and the cells were fixed with 4% paraformalydehide in the PBS (pH 7.4) for 10 min and permeabilized with 0.1% Triton X-100® for 10 min. The morphology of the cell nuclei was visualized by staining with the DNA intercalating dye Hoechst 33,342 (Riedel de Haen, Seelze, Germany, 5 μg/ml) for 30 min in the dark. The samples were washed with PBS, and actin filaments were stained with the green-fluorescent dye Phalloidin, fluorescein isothiocyanate labeled according to the manufacturer's procedure. After staining, the cells were washed with PBS and air-dried, and the cover-glasses were then fixed on the slide and observed using a 60× objective.

2.2.5. AFM study of cell morphology

2.2.5.1. Sample preparation (fixed and live cells). For AFM imaging of fixed cells, a dry-heat sterilized round glass coverslip (2r = 15 mm, Thermo Scientific, Menzel-Gläser, Braunschweig, Germany) was placed inside a 12-well plate (TPP, Trasadingen, Switzerland). For live cell imaging, coverslips were additionally coated with either a fibronectin or collagen solution prepared according to the manufacturer's procedure. 5 μg/cm^2 of fibronectin and collagen solution was used for coating the coverslips prior to cell attachment. Poly-L-lysine–coated coverslips were purchased and additionally utilized for attachment of cells to substrate (2*r* = 12 mm; BD Biosciences, Bedford, MA, USA). The cells were seeded at density of 4×10^5 cells per well and incubated overnight. Test formulation (i.e., LLCS solution in cell culture medium) was added to a final concentration of 0.5 mg/ml. Cells designed for fixation were 4 h post-treatment fixed with either 4% paraformaldehyde in PBS (pH 7.4) or ice-cold 96% ethanol (Kefo, Ljubljana, Slovenia) for 10 min. The same fixation protocol was used for control cells. Subsequently the cells were washed twice in phosphate-buffered saline and once in bidistilled water, and then air dried. Regarding live cell imaging, the suitability of each coating technique

was evaluated, and the most promising approach (i.e., coating with fibronectin) was used for all further live cell analysis.

2.2.5.2. AFM imaging of fixed cells. AFM imaging of fixed cells was performed using a Nanoscope IIIa multimode scanning probe microscope equipped with a J-type scanner (Veeco, Santa Barbara, CA, USA). Sharp silicon nitride cantilevers (MSCT, Veeco, Santa Barbara, CA, USA) with a spring constant of 0.1 N/m were used for imaging. Data were recorded at a scan rate of 3 Hz and stored in 512 × 512 pixel format. Images were processed using Nanoscope software. For optimal image quality of structural details, third-order flattening was applied.

2.2.5.3. AFM imaging of live cells. AFM imaging of living keratinocytes in PBS medium was conducted using a liquid imaging cell sealed with an O-ring in tapping mode. Silicon nitride cantilevers (PPP-BSI, Nanosensors, Wetlzar, Germany) with a spring constant of 0.1 N/m and resonance frequency of 28 kHz were used for imaging. Data were recorded at a scan rate of 1 Hz, stored in 512 × 512 pixel format and processed using Nanoscope software.

2.2.5.4. Measurement of keratinocyte rigidity. Sample preparation was the same as for the AFM imaging analysis. Probing of fixed cells was performed using sharp silicon-nitride cantilevers (MSCT, Veeco, Santa Barbara, CA, USA) with a nominal spring constant of 0.1 N/m.

For evaluation of live cell stiffness, spherical silicon oxide tips with diameter of 0.8 μm and a spring constant of 0.2 N/m were applied and the experiment was conducted in a PBS medium. The nanoindentation measurements involved recording the deflection-displacement curves at the nucleus area of the cells in order to avoid influence of the substrate stiffness on the elasticity results. At least three cells were tested on mechanical properties, and at least 20 curves per cell were collected.

2.2.5.5. Data analysis. The raw deflection curves were converted to force separation curves using the spring constant of the cantilevers. Such curves are further converted into force-deformation curves by identifying the contact point. In order to extract Young's modulus, the Hertz model was applied to analyze the force curves. Briefly, the Hertz theory neglects any adhesions between surfaces in contact, and therefore only approaching curves were used for elasticity calculation. This model in the case of a paraboidal indenter on a flat surface is given by the following Eq. (1):

$$F = \frac{4\sqrt{R_c}}{3}\frac{E}{1-\nu^2}\delta^{3/2} \quad (1)$$

where F is the force, R_c is the radius of the tip curvature, E is Young's modulus, ν is the Poisson ration of material (0.5 for soft biological samples), and δ is the deformation. Young's moduli were calculated from the linear slope of $F^{2/3}$ vs. deformation curves.

3. Results

3.1. Cell proliferation evaluation

The cell proliferation results as assessed by MTS metabolism following short (4 h) and long (24 h) exposure to the LLCS system at concentrations of 0.5, 1, 2, and 5 mg/ml are summarized in Fig. 1. Short (4 h) exposure to the LLCS system yielded high cell proliferation at all concentrations tested. Specifically, at the lowest concentration tested (0.5 mg/ml) the proliferation was the same as for the control (untreated cells). A decrease in cell proliferation was evident with increasing concentration even though the proliferation still remained high (i.e., 77.0 and 64.8% at 2 and 5 mg/ml, respectively). Prolongation of exposure time up to 24 h resulted in reduced cell proliferation compared to the control over the entire concentration range (% of viability ranged between 78.2% and 57.5% up to 2 mg/ml). The decline was the most

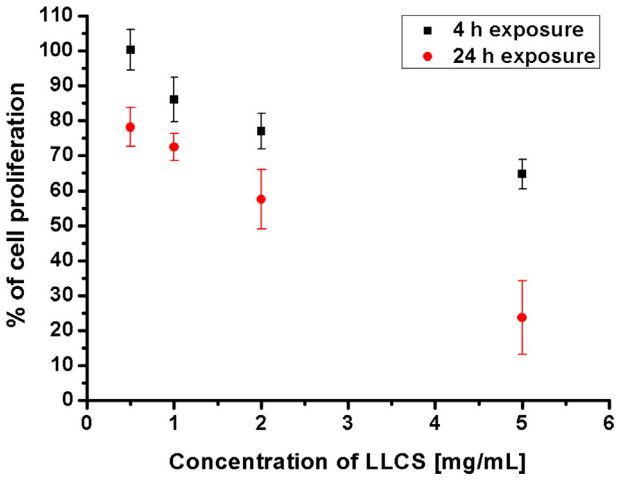

Fig. 1. Keratinocyte proliferation following 4 h and 24 h exposure to LLCS at different concentrations. The results are presented relative to the proliferation of untreated (control) cells. Data are expressed as mean ± SD (n = 6).

prominent at the highest concentration tested (5 mg/ml), with cell proliferation being 24%.

Cells were concurrently observed under an inverted phase-contrast microscope for a routine preliminary morphology check (Fig. 2). The MTS assay results correlate well with the alteration of the cell morphology in the culture. Namely, after 4 h exposure to the LLCS system at 0.5 mg/ml, keratinocytes resembled control cells in shape, number, and intercellular connections, whereas after 24 h a minority of cells lost their characteristic triangular shape (the cells became round with less-pronounced intercellular connections, but were still attached to the surface). The same morphology alterations, but then again at higher concentration (1 mg/ml), could be observed following 4 h exposure. Prominent changes such as elongated cell shape, missing interconnections, reduced cell number, and detached cells were observed starting at a concentration of 2 mg/ml or 1 mg/ml following 4 h or 24 h of treatment, respectively. These alterations were concentration- and time-dependent, until cell fragments were detected as tiny black dots at 5 mg/ml 24 h post treatment.

3.2. Fluorescence imaging

For detailed morphological evaluation, fluorescence micrographs of keratinocytes were conducted (Fig. 2). The control cells displayed a polygonal shape with oval or round nuclei and evenly distributed actin fibres along with numerous microfilament interconnections. Following 4 h of treatment at 0.5 mg/ml, the morphological features remained unchanged, whereas at 1 mg/ml there were subtle changes (i.e., absence of evident microfilaments together with intercellular connections that resulted in a distinct cell edge). This effect is typically connected to surfactants' impact on actin filaments (Kobiela et al., 2013). At a concentration of 2 mg/ml, the condensed actin fibres concentrated around nuclei, which resulted in more rounded cell morphology. The effect was significantly expressed at 5 mg/ml (demolished actin fibres concentrated around nuclei, and cells lost their characteristic shape and became round). Following 24 h of exposure, the absence of fine microfilament connections was already detected at the lowest concentration tested. With a concentration of 2 mg/ml, evident structural alterations of actin fibres concentrated around nuclei were observed (cells were round, stacked together, and randomly positioned).

3.3. AFM imaging of keratinocytes' morphological and rigidity alterations

3.3.1. Fixed cells' morphology and rigidity

The morphology of the control and treated keratinocytes fixed with

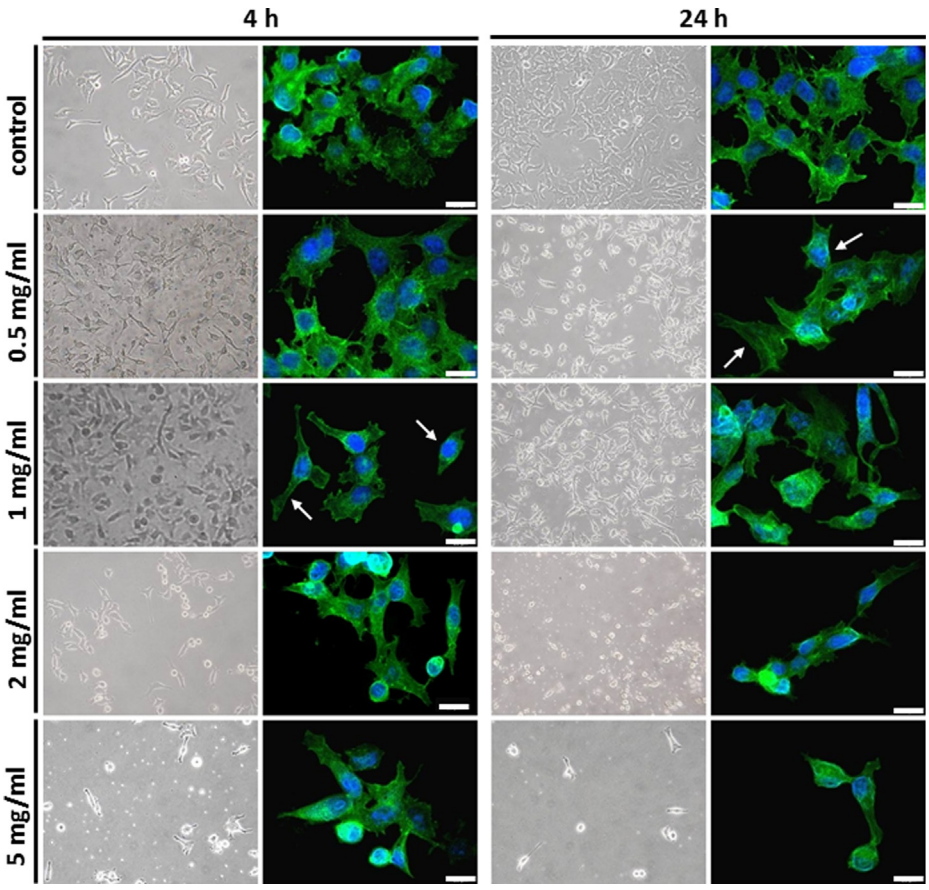

Fig. 2. Morphology of the keratinocytes following 4 h and 24 h exposure to LLCS as assessed by inverted light microscopy (left columns) and fluorescence microscopy (right columns) at various concentrations with respect to control cells (top row). Live-cell light transmission micrographs were taken using 20× magnification. The green and blue signals on fluorescence images are from Phalloidin and Hoechst 33342, respectively. The white arrows on the fluorescence images indicate morphological alterations (namely, the absence of microfilaments and round cell shape) observed at initial concentration (1 mg/ml and 0.5 mg/ml after 4 h and 24 h exposure, respectively). (For interpretation of the references to colour in this figure legend, the reader is referred to the web version of this article.)

ethanol and PFA is presented in Fig. 3. Topography information for the cells investigated is shown in the form of deflection images. They do not reflect true height variations, but, on the other hand, they are more sensitive to fine surface details useful for revealing the morphology ultrastructure (Irman et al., 2009; Pelling et al., 2005). The volcano-like depressions are visualized due to the dehydration of the cells induced by the fixation with ethanol (Fig. 3a and b) (Moloney et al., 2004). The nucleus appears to be collapsed during dehydration. This leads to formation of a prominent nuclear edge. During cell fixation through cross-linking of the plasma membrane with PFA (Fig. 3c and d) no depression, coating, or streaking effects occurred. Treatment with the LLCS system preserved domed and turgid cells with distinct areas of nucleus and cytoplasm (Fig. 3d), as in the case of the control group (Fig. 3c). Furthermore, treated cells maintained their characteristic polygonal shape. Surface alterations were evident as holes and represent commonly observed artifacts due to the fixation with PFA (Moloney et al., 2004).

Magnification of the cell membrane revealed small roundish protruding structures (Fig. 4a and b) that were observed for all cells fixed with PFA investigated, and filamentous structures (Fig. 5) were observed for LLCS-treated cells irrespective of the fixative used. Ultimately, AFM qualitative results did not reveal morphological signs of cells' cytotoxic effects, such as membrane invagination and rounding of the cells following keratinocyte exposure to the LLCS system. Quantitate structural information (height, roughness) are presented in in the Supplementary materials.

Fixation of keratinocytes with PFA was selected as suitable for estimation of the LLCS effect on the cell membrane structure because no generation of artefacts was induced by PFA (absence of depression, coating, or streaking). No correlation between the effect of the LLCS system and modifications in the shape and morphology of keratinocytes was determined.

In this study, local nanoindentation was performed on the keratinocytes' membrane to determine Young's modulus (E) as a measure of cell stiffness. Fig. 6 shows a representative force vs. deformation curve obtained on control and LLCS system–treated keratinocytes fixed with PFA. It should be noted that E is calculated from the slope of force $^{2/3}$ vs. deformation curve according to the Hertz model. Several parameters describing the mechanical properties of the cells must be specified. E of the cells, according to literature data, is dependent on their growth stage including the number of passage cycles, the number of growth days per passage cycle, and the cellular region selected for the AFM nanoindentation (Fung et al., 2011; Sokolov et al., 2006). In our case study, AFM nanoindentation was performed on young keratinocytes because three passage cycles were carried out. The growth period between the passage cycles was four days. In order to avoid influence of the substrate on the cell rigidity, we collected force curves at the nucleus region at various positions (Fig. 6b). This is consistent with the other literature data because E in the thicker cellular parts closer to the cell body (cytoplasmic and nucleus area) can be successfully ascertained by using the Hertz model (Leporatti et al., 2006; Lulevich et al., 2010).

It should be noted that elasticity measurements were conducted using the sharp AFM tip after fixation of cells with ethanol and PFA. According to the literature data, cell rigidity measurements were carried out with the various AFM sensors such as sharp tips and colloidal (spherical) probes (Berdyyeva et al., 2005; Kasas et al., 2005). In addition, we determined the practicability of the sharp AFM tips in determination of elasticity differences between the control and treated keratinocytes for the previously fixated cells.

We demonstrated that Young's moduli of the cells treated with LLCS decrease irrespective of the fixation procedure (Fig. 7); however, the stiffer membrane of keratinocytes fixed with ethanol is related to dehydration of the cells when compared to PFA-treated ones (Baker,

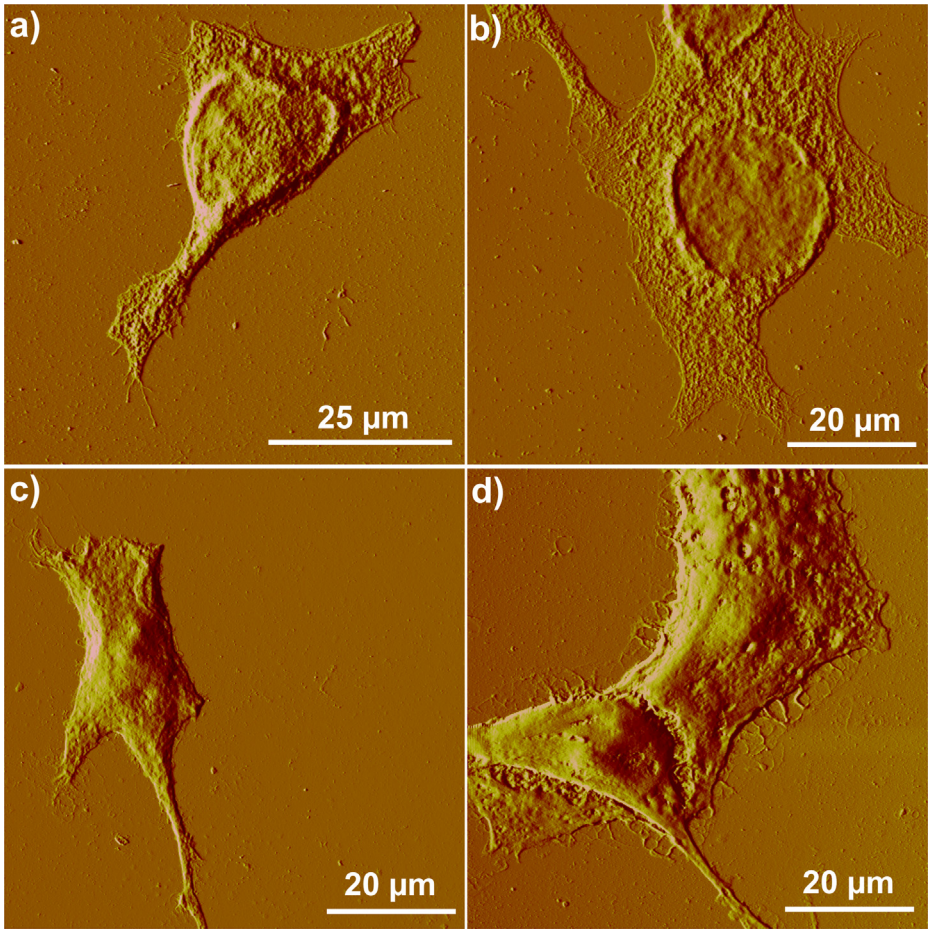

Fig. 3. Morphology of the control cells (left column) and cells treated with LLCS (right column) fixed with ethanol (a and b) or PFA (c and d).

1958; Rubin and Rottenberg, 1983). Overall, keratinocytes became more elastic after 4 h of exposure to the LLCS formulation.

Our results are also in good agreement with the other literature data regarding the elasticity of young keratinocytes in the nucleus area (Berdyyeva et al., 2005; Fung et al., 2011; Lulevich et al., 2010; Sokolov et al., 2006). It should be noted that a significant variations in Young's moduli at different points in the nucleus region of the cell membrane were observed. Such a result is consistent with the local heterogeneity of the cell membrane probed with the AFM tip.

3.3.2. Live cells' morphology and rigidity

We also applied the AFM technique to study how LLCS impacts live keratinocytes' properties. Topography images of cells with LLCS treatment were obtained and compared to the control group under the same environmental conditions. Keratinocytes were grown to confluence on the glass coverslips covered with either collagen or fibronectin and placed under the AFM. In case of collagen coated coverslips the keratinocytes' attachment was so loose that AFM imaging could not be performed as the cells were moving along with AFM tip, so only fibronectin coated coverslips were applicable for further live cell

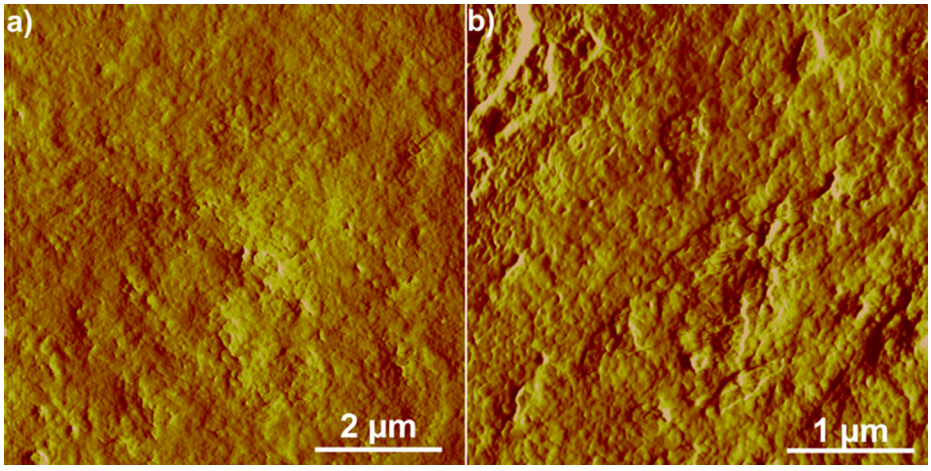

Fig. 4. Surface appearance of the control (a) and LLCS-treated cells (b) a typical granular structure is observed. Keratinocytes were fixed with PFA.

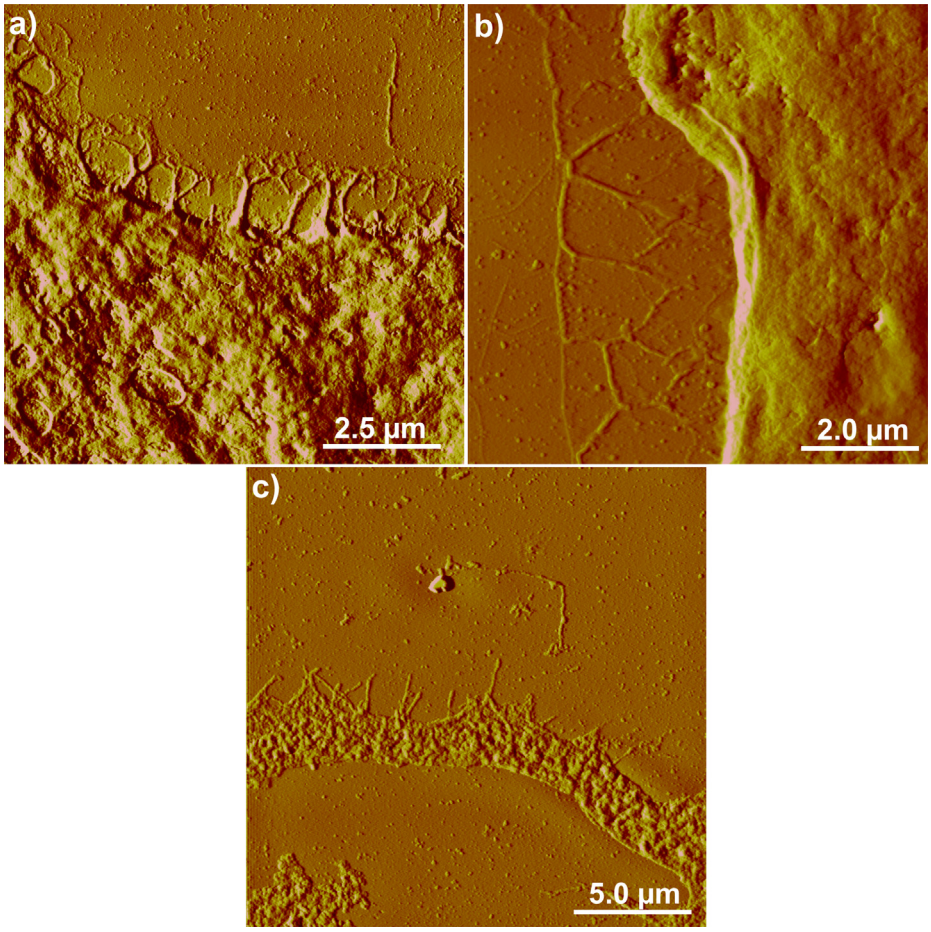

Fig. 5. Filamentous structures observed for LLCS-treated cells; keratinocytes fixed with PFA (a and b) and ethanol (c).

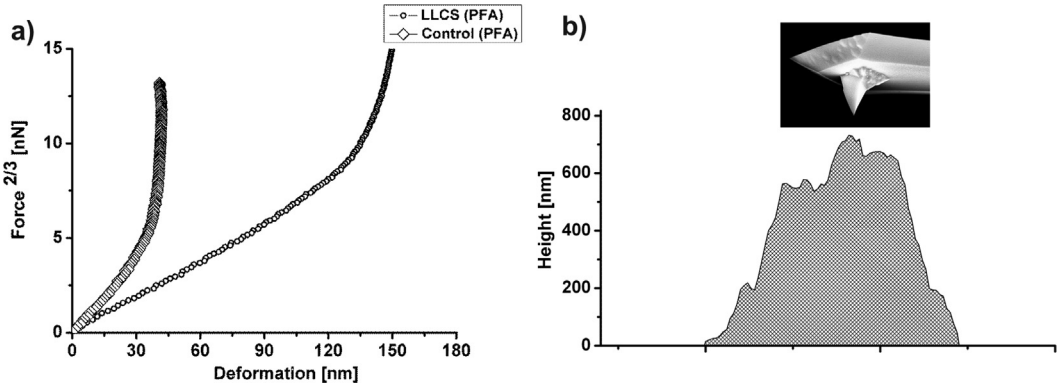

Fig. 6. (a) Force vs. deformation curves obtained on control cells and LLCS-treated cells fixed with PFA. (b) The height profile of the keratinocyte from the control group (fixed with PFA). The scheme additionally implies nuclear regions, where the single-point nanoindentation was performed.

analysis. Images were obtained in the phosphate buffer saline medium in order to keep cells in a near-natural state. The typical AFM height image of treated live keratinocytes with LLCS is shown in Fig. 8.

In the scan area of 60 × 60 µm^2, peripheral parts of keratinocytes were revealed with typical polygonal morphology and surface characteristics (presence of cytoskeletal fibers). No invaginations of the cell surface as a result of cytoskeletal modifications occurring in cytoplasm were detected after the exposure of keratinocytes to LLCS. Unfixed cells are very susceptible and undergo continuous dynamic changes to their cellular membranes during AFM scanning. Therefore, it was feasible to visualize only peripheral and cytoplasmic parts of the cells that had a height of less than 6 µm. The intact morphology of cells treated with LLCS visualized with AFM agrees well with the inverted light and fluorescence microscopy images (Fig. 2). The slightly increased roughness of the cells' surface can be related to scanning artefacts due to the soft nature of live keratinocytes.

The elasticity of live keratinocytes was also determined under physiological conditions at the nanoscale by using AFM nanoindentation. Mapping of rigidity was localized at the center of the cells to avoid the substrate effect of force measurements recorded at cell peripheral sites as well as tip slippage. Utilizing AFM-based single cell compression, the ability of live keratinocytes to resist external pressure and global rupturing forces was investigated after treatment with LLCS and compared with untreated ones. Force measurements were carefully

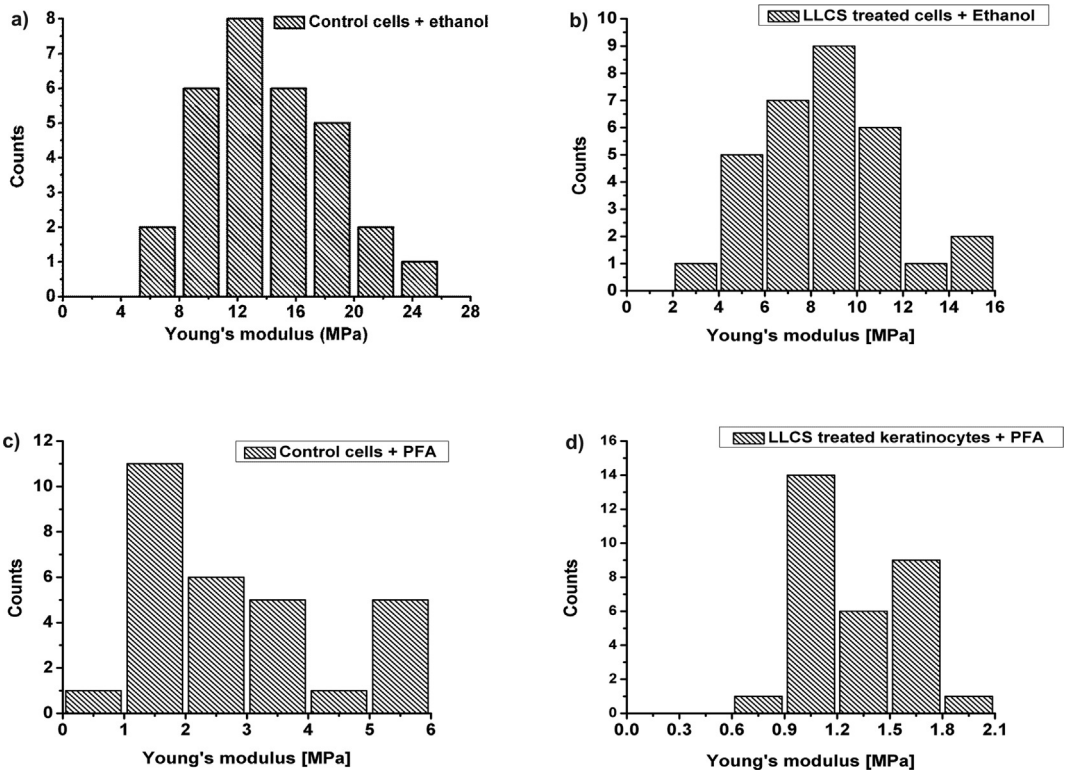

Fig. 7. Young's moduli of the control and treated groups of keratinocytes fixed with either ethanol (a and b) or PFA (c and d).

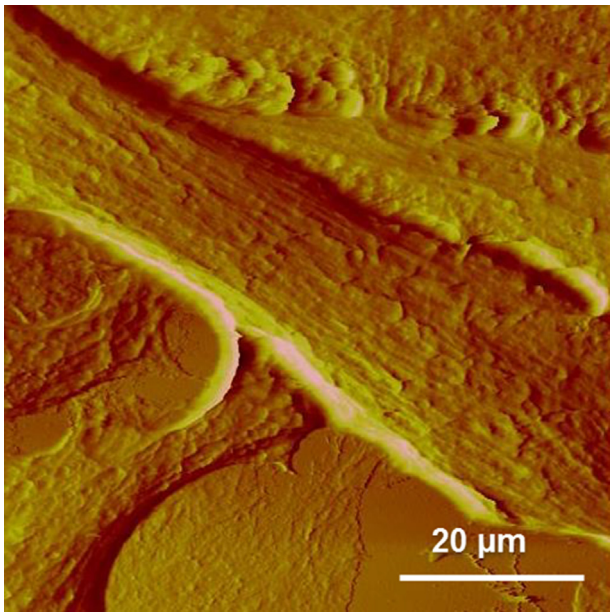

Fig. 8. Height image of a live keratinocyte's surface.

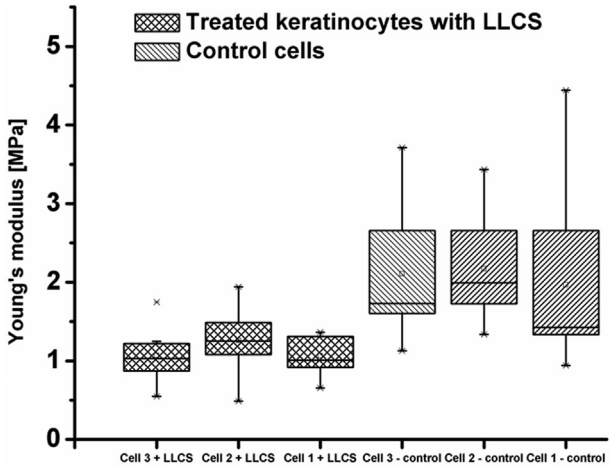

Fig. 9. Elasticity of live keratinocytes estimated before (control) and after treatment with LCCS.

conducted, with no membrane rupturing peaks in the force deformation profiles. Up to 20 force curves were collected and analyzed per cell. Only living keratinocytes tightly attached to fibronectin coverslips were used to assess their elasticity.

In our case, the calculated Young's modulus is a measure of mechanical resilience of live keratinocytes dictated by the cytoskeleton and membrane. To our knowledge, this is the first study in which the elasticity of keratinocytes was evaluated after treatment with LLCS. This system may have relevance in preventing the loss of tissue elasticity that results from rigidification of the extracellular matrix.

The results of Young's moduli are summarized in Fig. 9. The values range from 1.1 to 4.5 MPa for the untreated group, and from 0.6 to 2.8 MPa for treated cells. The AFM indentations of control cells resulted in a broad distribution of values for Young's modulus. It was interesting to observe that some keratinocytes yielded values that were about an order of magnitude larger than some cells in the same experiment, implying that cells behave heterogeneously regarding elasticity. Cells treated with LLCS showed a more concentrated distribution of Young's modulus, which is shifted toward lower values. Our results obtained for Young's modulus are in accordance to other literature data determining the elasticity of keratinocytes with AFM nanoindentation (Fung et al., 2011; Lulevich et al., 2010).

4. Discussion

4.1. LLCS impact on cell metabolic activity and morphology

A proliferation assay is a common test for cytotoxicity evaluation of various compounds because changes in metabolic activity imply early cell injury. A substance is determined to be a non-irritant or irritant when cell proliferation is above 85% or under 50%, respectively, based on *in vitro* skin irritation testing on reconstructed human epidermis (RHE) (Tornier et al., 2006). This requirement is also used for cosmetic product irritation assessment, with the cutoff value set at 50% of cell viability after 16 h exposure (Faller et al., 2002). Despite the greater sensitivity of cell culture lines in comparison to RHE (Welss et al., 2004), the limits provided are commonly accepted for interpretation of results; however, assessment of dermal acceptability taking these criteria into consideration is clearly much stricter.

Our previous study reported the development and structural characterization of lecithin-based lamellar liquid crystal delivery systems and offered an initial cytotoxicity assessment. The two systems tested (constant surfactant but various water/oil content) proved to be non-toxic because high cell proliferation (not less than 70%) was determined (Gosenca et al., 2013). Because AFM evaluation of keratinocytes' structural and elasticity alterations following LLCS application was the main focus of present study, a lamellar liquid system with the highest cell proliferation and less prominent declines among various concentrations tested (i.e., LLCS) was used as a model system. This choice was also made with the awareness that subtle but key alterations involved in cell response to an exposed agent may be disguised by evident structural derangement often observed following exposure to non-cytotoxic-doses (e.g., cell membrane changes detected due to modification of the lipid bilayer after non-toxic exposure of $HgCl_2$) (Lasalvia et al., 2011; Perna et al, 2007).

Along with the imaging techniques (inverted phase contrast plus fluorescence microscopy), a cell proliferation assay was performed to determine the compliant concentration of LLCS tested for further AFM study on keratinocytes. For the experimental setup it was necessary to dilute the LLCS system prior to cell treatment. Consequently, its inner lamellar structure was altered and resulted in the formation of a hydrophilic course emulsion (Gosenca et al., 2013). Nevertheless, the system retained short-range organization (IPM being enclosed within amphiphilic molecules, although the long-range structural arrangement was missing).

Following short-term (4 h) exposure, the cell proliferation was above the limit value of 85% at 0.5 and 1 mg/ml; at the lowest concentration tested, it was the same as for the control (Fig. 1). After long-term exposure (24 h), the cell proliferation was already below 50% at the lowest concentration tested, indicating concentration as well as a time-dependent effect of LLCS, nevertheless the cells were more susceptible to prolongation of exposure time than to concentration increasing. Most likely at higher concentration interactions of LLCS with cell membrane as discussed in details within Section 4.2 resulted in solubilization of cell membrane, and this effect occurred already at lower concentrations after long-term exposure due to increased contact time. The inverted phase-contrast and florescence microscopy images illustrated morphological changes of keratinocytes after 4 h at concentrations higher than 0.5 mg/ml. For these, normal cell growth was observed with well-spread, interconnected cells, evenly distributed actin fibers, and round nuclei, comparable to the control cells. At 1 mg/ml of LLCS, morphological alterations regarding cell shape and the number of intercellular connections were subtle and expressed in only a few cells. Significant cell morphology changes (i.e., elongated cell shape, fewer interconnections, reduced cell number, and cells detached from the surface) were observed at higher concentrations tested. Following 24 h of treatment, small changes in cell shape were observed using inverted phase-contrast microscopy at 0.5 mg/ml, and accompanied with actin fiber derangement detected by fluorescence imaging (Fig. 2). Similar alterations that were provoked at a higher LLCS concentration after short-term exposure have already been observed at lower concentrations after long-term exposure.

Based on cell proliferation and fluorescence imaging results, 0.5 mg/ml of LLCS following 4 h exposure was determined as a non-cytotoxic regime. For that reason further AFM study of keratinocytes' morphological and mechanical properties was performed following cell treatment at 0.5 mg/ml of LLCs for 4 h.

4.2. Mechanical properties of immobilized and live cells

The general concept of cell membrane structure includes a fluid assembly of amphiphilic lipids into a two-dimensional liquid crystalline structure with membrane fluidity defined as the ability of the structure to flow under an applied shear stress. It is governed by lipids (glycerophospholipids such as phosphatidylcholine) and membrane protein mobility (Goñi, 2014; Nicolson, 2014; Singer and Nicolson, 1972). However, the rigidity of human epithelial tissue increases with aging, and current literature data imply that individual epithelial cells also become considerably more rigid during aging *in vitro* (Berdyyeva et al., 2005). Therefore, AFM nanoindentation was for the most part oriented toward cell membrane stiffness evaluation. For this purpose, immobilized (i.e., PFA- and ethanol-fixed) and live cells were utilized as substrates investigated for LLCS impact. According to our results, the optimal immobilization condition was obtained by using PFA (4%, 10 min) because the keratinocytes' shape and morphology were preserved. In particular, the cell response following exposure to LLCS resulted in the formation of a prominent edge area (Fig. 3b) or nanofibrils (Fig. 5). The edge area was more emphasized with ethanol as a fixative (96%, 10 min) compared to the numerous separate and cross-linked filaments observed on keratinocytes fixed with PFA. The nanofibrillar structures observed have already been reported for keratinocytes' treatment with ZnO and TiO_2 nanoparticles. Such features are not cytotoxic modifications, but they are related to weakly connected and highly migrated cells in terms of communication channels (transport of molecules or organelles) (Kocbek et al, 2010).

Upon the movement of the AFM sensor toward the surface, the AFM probe subsequently sensed the superficial polysaccharide layer (glycocalyx), the cell membrane coupled with the network of F-actin fibers, and the deeper cell body (Sokolov, 2006). At the level of AFM deformation utilized (around 100 nm), the influence of underlying organelles is negligible (Leporatti et al., 2006). Because solubilization of the cell membrane did not occur during the fixation procedure with PFA, the rigidity of the keratinocytes obtained in this case study mainly reflects the elastic properties of the cell membrane.

The summary of our experimental findings with AFM nanoindentation was that keratinocytes are more elastic and homogeneous upon application of LLCS when compared to the control group. Such an effect does not correlate with degradation of the cytoskeleton because the shape and morphological features of the treated keratinocytes are preserved (Figs. 2 and 8). Moreover, decreased rigidity is detected for fixed and live keratinocytes. In the case of immobilized cells, more relevant results are related to the PFA procedure because lipids remain unfixed in comparison to ethanol, for which most of the membrane lipid compounds are dissolved. Regarding the nanoindentation procedure, it can be stated that the sharp AFM tip used is capable of detecting alteration in the membrane rigidity between the control and LLCS-treated cells regardless of the fixation procedure. Furthermore, live cells treated with LLCS remained in their native form (polygonal shape), and therefore its influence on the cells' cytoskeletal network can be excluded.

According to data from the literature, changes in cytoskeletal organization as a result of tumorigenesis (Buda and Pignatelli, 2004; Lindberg et al., 2008) or treatment with various agents (e.g., nocodazole (Pelling et al., 2007) and colchicine plus paclitaxel (Tsai et al., 1998) were elucidated. Under such conditions, the decreased elasticity

of the cells investigated is attributed to a lower concentration of F-actin fibers in the cytoskeletal structure. Keratinocyte treatment with anti-aging bioactive peptide resulted in decreased elastic modulus that correspond to the alteration in the arrangement of actin filaments as well (Kobiela et al., 2018). On the other hand, aging induces stiffening of the epithelial cells as a consequence of increased F-actin concentration in the cytoskeletal structure (Berdyyeva et al., 2005; Fung et al., 2011; Lulevich et al., 2010; Sokolov et al., 2006). Alteration of the cytoskeletal organizations leads to morphological and surface changes such as shape modifications, membrane invaginations, and roughness variations.

Then again, the molecular mechanism leading to softening effects on keratinocytes after exposure to LLCS has not been revealed yet. The possible explanation can be related to the specific chemical composition and structural organization of LLCS. It should be noted that the main constituents of the LLCS investigated are water, lecithin with phosphatidylcholine content not less than 94%, polyoxyethylene (20) sorbitan monooleate (Tween 80), and isopropyl myristate as a lipophilic solvent. Some authors have described a lipid-modulating or lipolytic effect of phosphatidylcholine following subcutaneous injection (Heron et al., 1982). As a result, the fluidity of the cell membrane is increased. Orally administered cell membrane phospholipids also naturally replace and stimulate removal of damaged membrane lipids; this approach is known as lipid replacement therapy, aiming to restore cellular function impaired during aging and in various clinical conditions (Nicolson and Ash, 2014). What is more, Selyutina et al. (2016) reported on glycyrrhizin′ (triterpenoid saponin) increased human erythrocytes′ membrane elasticity and narrowed distribution of elasticity modulus being in accordance with our observation. Effects were connected to glycyrrhizin interactions with biomembrane, namely extraction of cholesterol that accumulates in the lipid bilayer upon aging of cell membranes. In line with these results along with age-induced increased rigidity of epithelial cells, observed softening effect on keratinocytes after exposure to LLCS can possibly contribute to cell rejuvenation. Moreover, considering increased membrane permeability and thus facilitated drug penetration due to interactions with biomembranes (Selyutina et al., 2016), LLCS show optimal features to be implemented as novel carrier system for efficient dermal delivery of active substances in prophylaxis and therapy of (photo) aging induced skin damage. For example, antioxidant, though well recognized within current treatment of (photo) aging skin (Ramos-e-Silva et al., 2013), often have low skin bioavailability (Gašperlin and Gosenca, 2011). This drawback could be overcome by incorporation into LLCS that would potentially contribute to superior penetration into the skin to improve endogenous skin antioxidant system and at the same time rejuvenate rigid aged skin cells. However, it is important to consider barrier function of the skin *in vivo*, therefore LLCS was tested on the SC layer as a model membrane with results presented and discussed in Supplementary material. Briefly, AFM images of SC layer proved LLCS to penetrate deeper into SC, however additional experiments should be performed (e.g., further thorough AFM study of the LLCS treated SC plus *in vitro* permeation studies of incorporated antioxidants using, e.g., reconstructed human epidermis models) in order to unequivocally address the issue regarding LLCS *in vivo* performance.

Keeping to our observation, improved elasticity of the cell membrane of fixed and live keratinocytes can be explained with potential lecithin interaction from LLCS with the membrane inducing hypoviscosity of the lipids and enhancing membrane fluidity under compression. The effect is based on replacement of the phosphatidylcholine molecule located preferentially on the outer leaflet of the cell membrane surface (Nicolson and Ash, 2014). The Saffman–Delbrück model is the main one describing membrane fluidity, according to which area per lipid tail and presence of van der Waals and hydrogen bonds are the major contributing factors to the membrane diffusion coefficient. Viscosity of cell membrane is a measure of intermolecular interaction intensity. These are related to presence of van der Waals, hydrogen, and electrostatic bonds, which hold lipids together. LLCS-induced hypoviscosity of the cell membrane is confirmed with reduced values of E when compared to control cells. Considering the finite viscosity calculations given by the Saffman–Delbrück model (Seu et al., 2006), lower viscosity results in a higher diffusion coefficient of lipids in the membrane, and consequently improved fluidity. Hypoviscosity induced by phosphatidylcholine can be attributed to its lipid replacement effect (Nicolson and Ash, 2014) and is in agreement with the reported membrane lipid diffusion coefficient after the addition of phosphatidylcholine derivatives (Espinosa et al., 2011; Seu et al., 2006). With awareness of the cell membrane structure and dynamic (Goñi, 2014; Nicolson, 2014; van Meer et al., 2008) along with lipid bilayer nanomechanics (Garcia-Manyes et al., 2010) complexity, our hypothesis is that specific interactions between acyl chains of cell membrane phosphatidylcholine and those of LLCS induce the hypoviscosity observed, however lipidomic characterization (Dalmaua et al., 2018) should be performed to strengthen and complete our study. Even so plus recognizing importance of each LLCS component′s features, the phospholipid used for LLCS preparation has a phosphatidylcholine content not less than 94% w/w with the fatty acids of the two acyl groups being palmitic (15%), stearic (3%), oleic and isomers (12%), linoleic (62%), and linolenic (5%) according to the manufacturer′s specification. Indeed, phosphatidylcholines in the cell membrane are typically unsaturated, yet additional incorporation of mostly unsaturated acyl chains resulted in weaker van der Waals interactions, consequently increasing the acyl chain volume in conjunction with diffusion. Moreover, cholesterol, universally present in the cell membrane, is known to promote the formation of highly ordered membrane domains with saturated lipids due to stronger van der Waals interactions between the acyl chains, thus increasing their effective length and decreasing the acyl chain volume (Filipov et al., 2003; Mouritsen and Zuckermann, 2004); Róg et al., 2009) Conversely, domains rich in unsaturated lipids, especially with a double bond in the middle, specific to our system investigated, have higher fluidity despite its presence (Martinez-Seara et al., 2008). In addition, it is stressed that the presence of water in the LLCS system potentially contributes to elevation of the lateral diffusion of lipids. The effect is governed by an increase in the lipid headgroup area and consequently a decrease in the effective hydrocarbon chain length of the lipids (Filippov et al., 2003).

5. Conclusion

Within this study, AFM was introduced to determine elasticity and morphological features of keratinocytes after exposure to a LLCS. The entire study was performed at non-toxic concentrations of LLCS (i.e., exhibiting no evident effect on cell metabolic activity or morphological features as determined by the cell proliferation assay and light plus fluorescence imaging). AFM imaging also proved the structural integrity of the cells tested. With this in mind, AFM measurements of cell elasticity represent a relevant hallmark of the first cell response to LLCS treatment. Specifically, improved elasticity of immobilized and live cells was determined as Young′s moduli decreased. We strongly believe that the structural composition of the LLCS tested is crucial in increased cell membrane elasticity in the keratinocytes observed, and therefore an extensive study oriented toward an LLCS effect on fibroblasts using Raman spectroscopy as a complementary method to AFM is in progress. Overall, the results presented in this study indicate the biological acceptability of the system tested with great potential for further development and potential use for aged skin treatment, among other applications.

Declaration of Competing Interest

The authors declare that they have no known competing financial interests or personal relationships that could have appeared to influence the work reported in this paper.

Acknowledgement

Funding: The authors acknowledge financial support from the Slovenian Research Agency, Slovenia (research core funding, No. P1-0189).

Appendix A. Supplementary material

Supplementary data to this article can be found online at https://doi.org/10.1016/j.ijpharm.2019.118712.

References

Alsteens, D., Gaub, H.E., Newton, R., Pfreundschuh, M., Gerber, C., Müller, D.J., 2017. Atomic force microscopy-based characterization and design of biointerfaces. Nat. Rev. Mater. 2 (5), 17008.
Baker, J.R., 1958. Principles of Biological Microtechnique: A Study of Fixation and Dyeing. Methuen and Co., Ltd., London.
Berdyyeva, T., Woodworth, C.D., Sokolov, I., 2005. Human epithelial cells increase their rigidity with ageing in vitro: direct measurements. Phys. Med. Biol. 50, 81–92.
Buda, A., Pignatelli, M., 2004. Cytoskeletal network in colon cancer: from genes to clinical application. Int. J. Biochem. Cell Biol. 36 (5), 759–765.
Coceano, G., Yousafzai, M.S., Ma, W., Ndoye, F., Venturelli, L., Hussain, I., Bonin, S., Niemela, J., Scoles, G., Cojoc, D., Ferrari, E., 2016. Investigation into local cell mechanics by atomic force microscopy mapping and optical tweezer vertical indentation. Nanotechnology 27 (6), 065102. https://doi.org/10.1088/0957-4484/27/6/065102.
Dalmaua, N., Andrieu-Abadieb, N., Taulera, R., Bedia, C., 2018. Phenotypic and lipidomic characterization of primary human epidermal keratinocytes exposed to simulated solar UV radiation. J. Dermatol. Sci. 92, 97–105.
Drvenica, I.T., Bukara, K.M., Ilić, V. Lj., Mišić, D.M., Vasić, B.Z., Gajić, R.B., Đorđević, V.B., Veljović, Đ.N., Belić, A., Bugarski, B.M., 2016. Biomembranes from slaughterhouse blood erythrocytes as prolonged release systems for dexamethasone sodium phosphate. Biotechnol. Prog. 32 (4), 1046–1055.
Espinosa, G., Lopez-Montero, U., Monroy, F., Langevin, D., 2011. Shear rheology of lipid monolayers and insights on membrane fluidity. PNAS 108 (15), 6008–6013.
Faller, C., Brachera, M., Damib, N., Roguet, R., 2002. Predictive ability of reconstructed human epidermis equivalents for the assessment of skin irritation of cosmetics. Toxicol. In Vitro 16, 557–572.
Filipov, A., Orädd, G., Lindblom, G., 2003. The effect of cholesterol on the lateral diffusion of phospholipids in oriented bilayers. Biophys. J. 84 (5), 3079–3086.
Filippov, A., Orädd, G., Lindblom, G., 2003. Influence of cholesterol and water content on phospholipid lateral diffusion in bilayers. Langmuir 19, 6397–6400.
Fung, C.K.M., Seiffert-Sinha, K., Lai, K.W.C., Yang, R., Panyard, D., Zhang, J., Xi, N., Sinha, A.A., 2010. Investigation of human keratinocyte cell adhesion using atomic force microscopy. Nanomed. Nanotech. Biol. Med. 6, 191–200.
Fung, C.K.M., Xi, N., Yang, R., Seiffert-Sinha, K., Ali, K.W.C., Sinha, A.A., 2011. Quantitative analysis of human keratinocyte cell elasticity using atomic force microscopy (AFM). IEEE T. Nanobiosci. 10, 9–14.
Garcia, P.D., Garcia, R., 2018. Determination of the elastic moduli of a single cell cultured on a rigid support by force microscopy. Biophys. J. 114 (12), 2923–2932.
Garcia-Manyes, S., Redondo-Morata, L., Oncins, G., Sanz, F., 2010. Nanomechanics of lipid bilayers: head or tails? J. Am. Chem. Soc. 132, 12874–12886.
Gašperlin, M., Gosenca, M., 2011. Main approaches for delivering antioxidant vitamins through the skin to prevent skin ageing. Expert Opin. Drug Deliv. 8 (7), 905–919.
Gibbs, S., 2009. In vitro irritation models and immune reactions. Skin Pharmacol. Physiol. 22, 103–113.
Goñi, F.M., 2014. The basic structure and dynamics of cell membranes: an update of the singer-nicolson model. BBA 1838, 1467–1476.
Gosenca, M., Bešter-Rogač, M., Gašperlin, M., 2013. Lecithin based lamellar liquid crystals as a physiologically acceptable dermal delivery system for ascorbyl palmitate. Eur. J. Pharm. Sci. 50, 114–122.
Hayashi, K., Iwata, M., 2015. Stiffness of cancer cells measured with an AFM indentation method. J. Mech. Behav. Biomed. Mater. 49, 105–111.
Hazen, M.J., Fernández Freire, P., Pérez Martín, J.M., Peropadre, A., Herrero, O., López, C., Labrador, V., 2010. The Importance of Microscopic Analysis for Accurate Interpretation of Chemical-Induced Cytotoxicity. In: Méndez-Vilas, A., Díaz, J. (Eds.), Microscopy: Science, Technology, Applications and Education, Vol. 3. Formatex Research Center, Badajoz, pp. 2145–2153.
Heron, D.S., Shinitzky, M., Samuel, D., 1982. Alleviation of drug withdrawal symptoms by treatment with a potent mixture of natural lipids. Eur. J. Pharmacol. 83, 253–261.
Irman, Š., Škarabot, M., Muševič, I., Rozman, B., Božič, B., 2009. In vitro model of annexin A5 Crystallization on nature phospholipid bilayers observed by atomic force microscopy. Autoimmunity 42, 414–423.
Kasas, S., Wang, X., Hirling, H., Marsault, R., Huni, B., Yersin, A., Regazzi, R., Grenningloh, G., Riederer, B., Forro, L., Dietler, G., Catsicas, S., 2005. Superficial and deep changes of cellular mechanical properties following cytoskeleton disassembly. Cell Motil. Cytoskel. 62, 124–132.
Kobiela, T., Lelen-Kaminska, K., Stepulak, M., Lekka, M., Malejczyk, M., Arct, J., Majewski, S., 2013. The influence of surfactants and hydrolyzed proteins on keratinocytes viability and elasticity. Skin Res. Technol. 19, 200–208.
Kobiela, T., Milner-Krawczyk, M., Pasikowska-Piwko, M., Bobecka-Wesołowska, K., Eris, I., Święszkowski, W., Dulinska-Molak, I., 2018. The effect of anti-aging peptides on mechanical and biological properties of hacat keratinocytes. Int. J. Pept. Res. Ther. 24, 577–587.
Kocbek, P., Teskač, K., Kreft, M., Kristl, J., 2010. Toxicological aspects of long-term treatment of keratinocytes with ZnO and TiO_2 nanoparticles. Small 17, 1908–1917.
Kristl, J., Teskac Plajnšek, K., Erdani Kreft, M., Janković, J., Kocbek, P., 2013. Intracellular trafficking of solid lipid nanoparticles and their distribution between cells through tunneling nanotubes. Eur. J. Pharm. Sci. 50, 139–148.
Lasalvia, M., Perna, G., Mezzenga, E., Migliorini, E., Lazzarino, M., Abbate, N.L., Capozzi, V., 2011. Atomic force microscopy investigation of morphological changes in living keratinocytes treated with $HgCl_2$ at not cytotoxic doses. J. Microsc. 243 (1), 40–46.
Leporatti, S., Gerth, A., Kohler, G., Kohlstrunk, B., Hauschildt, S., Donath, E., 2006. Elasticity and adhesion of resting and lipopolysaccharide-stimulated macrophages. FEBS Lett. 580, 450–454.
Li, M., Liu, L., Xu, X., Xing, X., Dang, D., Xi, N., Wang, Y., 2018. Nanoscale characterization of dynamic cellular viscoelasticity by atomic force microscopy with varying measurement parameters. J. Mech. Behav. Biomed. Mater. 82, 193–201.
Lindberg, U., Karlsson, R., Lassing, I., Schutt, C.E., Hoglund, A.S., 2008. The microfilament system and malignancy. Semin. Cancer Biol. 18, 2–11.
Lulevich, V., Yang, H., Isseroff, R.R., Gang-yu, L., 2010. Single cell mechanics of keratinocyte cells. Ultramicroscopy 110, 1435–1442.
Luo, Q., Kuang, D., Zhang, B., Song, G., 2016. Cell stiffness determined by atomic force microscopy and its correlation with cell motility. BBA 186o (9), 1953–1960.
Makai, M., Csányi, E., Németh, Z., Pálinkás, J., Erős, I., 2003. Structure and drug release of lamellar liquid crystals containing glycerol. Int. J. Pharm. 256 (1–2), 95–107.
Martinez-Seara, H., Róg, T., Pasenkiewicz-Gierula, M., Vattulainen, I., Karttunen, M., Reigada, R., 2008. Interplay of unsaturated phospholipids and cholesterol in membranes: effect of the double-bond position. Biophys. J. 95, 3295–3305.
Maver, U., Velnar, T., Gaberšček, M., Planinšek, O., Finšgar, M., 2016. Recent progressive use of atomic force microscopy in biomedical applications. Trends Anal. Chem. 80, 96–111.
Moloney, M., MsDonnell, L., O'Shea, H., 2004. Atomic force microscopy of bhk-21 cells: an investigation of cell fixation techniques. Ultramicroscopy 100, 153–161.
Mouritsen, O.G., Zuckermann, M.J., 2004. What's so special about cholesterol? Lipids 39 (11), 1101–1113.
Müller-Goymann, C.C., 2004. Physicochemical characterization of colloidal drug delivery systems such as reverse micelles, vesicles, liquid crystals and nanoparticles for topical administration. Eur. J. Pharm. Biopharm. 58, 343–356.
Nicolson, G.L., 2014. The fluid-mosaic model of membrane structure: still relevant to understanding the structure, function and dynamics of biological membranes after more than 40 years. BBA 1838, 1451–1466.
Nicolson, G.L., Ash, M.E., 2014. Lipid replacement therapy: a natural medicine approach to replacing damaged lipids in cellular membranes and organelles and restoring function. BBA 1838, 1657–1679.
Pelipenko, J., Kocbek, P., Govedarica, B., Rošic, R., Baumgartner, S., Kristl, J., 2013. The topography of electrospun nanofibers and its impact on the growth and mobility of keratinocytes. Eur. J. Pharm. Biopharm. 84, 401–411.
Pelling, A.E., Dawson, D.W., Carreon, D.M., Christiansen, J.J., Shen, R.R., Teitell, M.A., Gimzewski, J.K., 2007. Distinct contributions of microtubule subtypes to cell membrane shape and stability. Nanomedicine NBM 3, 43–52.
Pelling, A.E., Li, Y., Shi, W., Gimzewski, J.K., 2005. Nanoscale visualization and characterization of *myxococcus xanthus* cells with atomic force microscopy. Proc. Natl. Acad. Sci. 102, 6484–6489.
Perna, G., Lastella, M., Lasalvia, M., Mezzenga, E., Capozzi, V., 2007. Raman spectroscopy and atomic force microscopy study of cellular damage in human keratinocytes treated with $HgCl_2$. J. Mol. Struct. 834, 182–187.
Ramos-e-Silva, M., Ribeiro Celem, L., Ramos-e-Silva, S., Fucci-da-Costa, A.P., 2013. Anti-aging cosmetics: Facts and controversies. Clin. Dermatol. 31, 750–758.
Róg, T., Pasenkiewicz-Gierula, M., Vattulainen, I., Karttunen, M., 2009. Ordering effects of cholesterol and its analogues. BBA 1788, 97–121.
Rubin, E., Rottenberg, H., 1983. Ethanol and biological membranes: injury and adaptation. Pharmacol. Biochem. Behav. 18, 7–13.
Savić, S., Weber, C., Savić, M.M., Müller-Goymann, C., 2009. Natural surfactant-based topical vehicles for two model drugs: influence of different lipophilic excipients on in vitro/in vivo skin performance. Int. J. Pharm. 381, 220–230.
Selyutina, O.Yu., Polyakov, N.E., Korneev, D.V., Zaitsev, B.N., 2016. Influence of glycyrrhizin on permeability and elasticity of cell membrane: perspectives for drugs delivery. Drug Deliv. 23 (3), 848–855.
Seu, K.J., Cambera, L.R., Everly, R.M., Hovis, J.S., 2006. Influence of lipid chemistry on membrane fluidity: tail and headgroup interactions. Biophys. J. 91, 3727–3735.
Singer, S.J., Nicolson, G.L., 1972. The Fluid Mosaic Model of the Structure of Cell Membrane. Science 175 (4023), 720–731.
Sitterberg, J., Özcetin, A., Ehrhardt, C., Bakowsky, U., 2010. Utilising atomic force microscopy for the characterisation of nanoscale delivery systems. Eur. J. Pharm. Biopharm. 74, 2–13.
Sokolov, I., 2006. Atomic Force Microscopy in Cancer Cell Research. In: Nalwa, H.S., Webster, T. (Eds.), Cancer Nanotechnology. American Scientific Publishers, Los Angeles, pp. 1–17.
Sokolov, I., Dokukin, M.E., Guz, N.V., 2013. Method for quantitative measurements of the elastic modulus of biological cells in AFM indentation experiments. Methods 60, 202–213.
Sokolov, I., Iyer, S., Woodworth, C.D., 2006. Recovery of elasticity of aged human epithelial cells in vitro. Nanomed.-Nanotechnol. 2, 31–36.
Takahashi, N., Higashi, K., Ueda, K., Yamamoto, K., Moribe, K., 2018. Determination of non-spherical morphology of doxorubicin-loaded liposomes by atomic force microscopy. J. Pharm. Sci. 107 (2), 717–726.

Tornier, C., Rosdy, M., Maibach, H.I., 2006. In vitro skin irritation testing on reconstituted human epidermis: reproducibility for 50 chemicals tested with two protocols. Toxicol. In Vitro 20 (4), 401–416.
Tsai, M.A., Waugh, R.E., Keng, P.C., 1998. Passive mechanical behavior of human neutrophils: effects of colchicine and paclitaxel. Biophys. J. 74, 3282–3291.
van Meer, G., Voelker, D.R., Feigenson, G.W., 2008. Membrane lipids: where they are and how they behave. Nat. Rev. Mol. Cell Biol. 9 (2), 112–124.
van Smeden, J., Janssens, M., Gooris, G.S., Bouwstra, J.A., 2014. The important role of stratum corneum lipids for the cutaneous barrier function. BBA 1841, 295–313.
Welss, T., Basketter, D.A., Schroder, K.R., 2004. In vitro skin irritation: facts and future. state of the art review of mechanisms and models. Toxicol. In Vitro 18, 231–243.
Zemla, J., Danilkiewicz, J., Orzechowska, B., Pabijan, J., Seweryn, S., Lekka, M., 2018. Atomic force microscopy as a tool for assessing the cellular elasticity and adhesiveness to identify cancer cells and tissues. Semin. Cell Dev. Biol. 73, 115–124.